Applied Physics Letters

High gain and high ultraviolet/visible rejection ratio photodetectors using p-GaN/AlGaN/GaN heterostructures grown on Si

Cite as: Appl. Phys. Lett. **117**, 071101 (2020); https://doi.org/10.1063/5.0011685
Submitted: 24 April 2020 . Accepted: 05 July 2020 . Published Online: 17 August 2020

Qifeng Lyu, Huaxing Jiang, and Kei May Lau

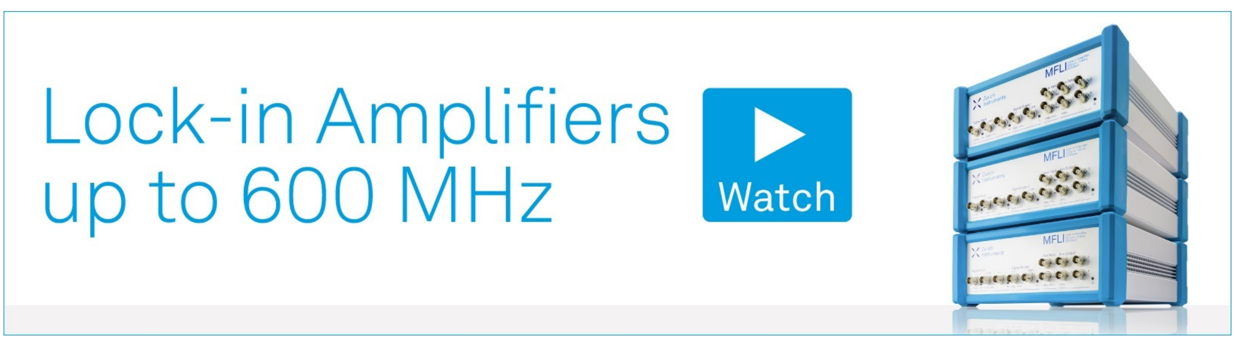

High gain and high ultraviolet/visible rejection ratio photodetectors using p-GaN/AlGaN/GaN heterostructures grown on Si

Cite as: Appl. Phys. Lett. **117**, 071101 (2020); doi: 10.1063/5.0011685
Submitted: 24 April 2020 · Accepted: 5 July 2020 ·
Published Online: 17 August 2020

Qifeng Lyu, Huaxing Jiang, and Kei May Lau[a)]

AFFILIATIONS

Department of Electronic and Computer Engineering, Hong Kong University of Science and Technology, Clear Water Bay, Kowloon, Hong Kong

[a)]Author to whom correspondence should be addressed: eekmlau@ust.hk. **Tel.:** 852-235-87049. **Fax:** 852-235-81485.

ABSTRACT

We report high performance ultraviolet (UV) photodetectors (PDs) based on p-GaN-gated AlGaN/GaN heterostructures grown on silicon substrates. Benefitting from the high electrical gain resulting from the transistor-like operation of the device, a photocurrent as high as 4.8 mA/mm was achieved with UV illumination. Due to the effective depletion of the two-dimensional electron gas at the AlGaN/GaN heterointerface via a p-GaN optical gate, the dark current was suppressed to below 3×10^{-8} mA/mm. A high photo-to-dark current ratio over 10^8 and a high responsivity of 2×10^4 A/W were demonstrated in the device. Moreover, with a cutoff wavelength of 395 nm, the PDs exhibited an ultrahigh UV-to-visible rejection ratio of over 10^7. Limited by a persistent photoconductivity effect, the rise time and fall time of the device frequency response were measured to be 12.2 ms and 8.9 ms, respectively. The results suggest the potential of the proposed PDs for high-sensitivity UV detection.

Ultraviolet (UV) photodetectors (PDs) have been widely employed in many applications such as aerospace engineering, ozone sensing, flame detection, and advanced communications.[1] As a direct wide bandgap semiconductor with excellent thermal and chemical stabilities, GaN has attracted extensive research interest for fabricating visible-blind UV PDs.[2] Various device structures, for instance, p–i–n,[3] metal–semiconductor–metal (MSM),[4] and Schottky diodes,[5] have been explored for GaN UV PDs. In addition to the conventional PD configurations, photoconductors consisting of an AlGaN (or InAlN)/GaN heterostructure, which is typically used in high electron mobility transistors (HEMTs), have also drawn great attention for UV detection.[6,7] Because of a high-density two-dimensional electron gas (2DEG) forming a conductive channel at the heterojunction interface, an ultrahigh photoresponsivity and high photocurrent are usually observed in the HEMT-based UV PDs. However, the existence of the 2DEG channel[8] also resulted in high dark currents (at the same order of the photocurrent) in these devices,[6,9,10] which decrease the detectivity and increase the power consumption. To suppress the dark current, the 2DEG channel was either depleted by adding a negatively-biased transparent metal gate[7,11] or floating p-GaN optical gate on the AlGaN barrier,[12–14] or partial removal of the AlGaN barrier leaving an i-GaN channel in between.[15–17] Among these approaches, HEMT-based PDs with a p-GaN optical gate have shown great promise.[12] However, all the reported HEMT-based PDs with p-GaN optical gates were demonstrated on sapphire substrates rather than on larger-size-available Si substrates with potentially lower cost.[12–14] Moreover, the dark currents in the reported devices, affected by the fabrication process and material epitaxy quality, are still not as low as that in HEMT-based PDs with a selectively removed AlGaN barrier structure.[16,17]

In this study, we report high-performance UV PDs based on p-GaN/AlGaN/GaN heterostructures grown on cost-effective silicon substrates. The device exhibits an ultralow dark current of 29 pA/mm and a large photocurrent of 4.8 mA/mm under a 365-nm light illumination, leading to an extremely high photo-to-dark current ratio of over 10^8 and a high responsivity of 2×10^4 A/W. With a cutoff wavelength of 395 nm, a large UV-to-visible rejection of $\sim 10^7$ is also achieved in the device. The gain mechanism of the PDs is discussed through the observation of the incident light intensity-controlled phototransistor operations. The time-domain photoresponse of the device is also investigated.

The p-GaN/AlGaN/GaN heterostructures used in this work, typically for p-GaN gate high electron mobility transistor application,[18] were grown on a 6-in. Si (111) substrate by metal organic chemical vapor deposition. The epilayers, from bottom to top, consist of a 5-μm high-resistivity GaN buffer, a 400-nm i-GaN layer, a 10-nm $Al_{0.2}Ga_{0.8}N$ barrier, and a 70-nm p-GaN cap layer with a Mg doping concentration of $\sim 5 \times 10^{19}\,cm^{-3}$. The hole concentration in the p-GaN layer is determined to be $\sim 1 \times 10^{18}\,cm^{-3}$ by the Hall measurement. The device structure, shown in Fig. 1(a), features a p-GaN stripe centering between two Ohmic electrodes, mimicking a transistor with an optical gate positioned between the source and drain electrodes. The p-GaN optical gate length ($L_{p\text{-}GaN}$) is 5 μm, the width (W) is 100 μm, and the distance between the electrode edge and the p-GaN edge (L_{AC}) is 1.5 μm on each side (access regions). Therefore, the total absorption area of the PD is 8 μm $\times$ 100 μm and the p-GaN optical gate area is 500 μm^2. Figure 1(b) illustrates the energy band diagram of the p-GaN/AlGaN/GaN heterostructures at thermal equilibrium. The device fabrication started with p-GaN patterning using inductively coupled plasma (ICP) dry etching to form a p-GaN stripe as an optical gate. Then, the Ohmic-contact electrodes were formed on the exposed $Al_{0.2}Ga_{0.8}N$ barrier using Ti (20 nm)/Al (150 nm)/Ni (50 nm)/Au (80 nm) metal stacks annealed at 850 °C for 30 s in nitrogen ambient, followed by the device isolation using fluorine ion implantation. The device was passivated with a 50-nm SiO_2 layer via plasma-enhanced chemical vapor deposition at 300 °C to decrease the trap density on the etching-exposed AlGaN surface and increase the 2DEG density in the access regions.[19] Finally, the pad metal was formed on the Ohmic electrodes using a Ni (20 nm)/Au (200 nm) metal stack. The photoresponsivity measurements were performed using a semiconductor device analyzer and a UV light emitting diode (LED) (Nichia NCSU276AT-0365) with a center emission wavelength of 365 nm and a narrow full width at half maximum of 16 nm. The PD photoresponse as a function of wavelength was measured using a spectroscope with a Xe lamp (broad band source) at room temperature. The intensity of the incident light from the LED was calibrated using a commercial Si photodetector (Centronic OSD 35–7X). The time domain response of the PD was characterized through the illumination of the 365-nm UV LED switched by a Si power transistor and measured using a Tektronix oscilloscope with a 100-MHz bandwidth.

Figure 2(a) compares the dark and photocurrent (normalized to the p-GaN optical gate width W; the same as below unless otherwise specified) under the 365-nm UV LED illumination of the PD as a function of the bias between the Ohmic electrodes. Benefitting from the effective depletion of the 2DEG underneath the p-GaN optical gate, the PD shows an ultralow dark current of $\sim 2.9 \times 10^{-8}$ mA/mm,

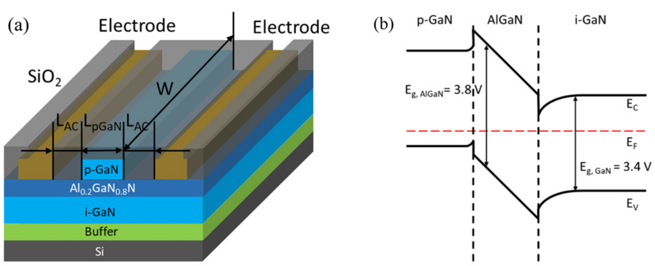

FIG. 1. (a) Schematic of the fabricated PDs in this work. $L_{p\text{-}GaN}$ is 5 μm, L_{AC} is 1.5 μm, and W is 100 μm. (b) The energy band diagram of the p-GaN/AlGaN/GaN heterostructures at thermal equilibrium.

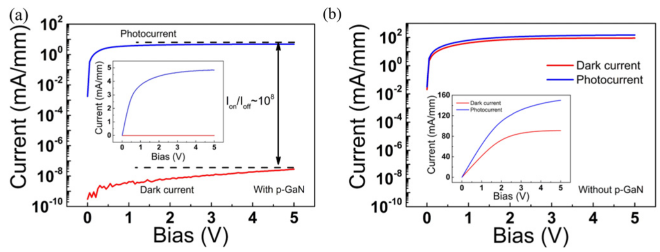

FIG. 2. Photo and dark currents of PDs (a) with and (b) without the p-GaN optical gate. The inset is the linear plot of the photo and dark currents.

while under the UV illumination with an intensity of 12 mW/cm^2, a photocurrent as high as 4.8 mA/mm can be measured in the device with a 5-V bias. As a result, an extremely high photo-to-dark current ratio of 1.7×10^8 is achieved in the PD. To reveal the reason for such a high photo-to-dark current ratio in our device, the photoresponse of a PD without the p-GaN optical gate on the same sample was measured for comparison, as shown in Fig. 2(b). Due to the formation of the conduction channel of the restored 2DEG after the p-GaN removal, the PD without the p-GaN optical gate shows a high dark current of 90 mA/mm under a 5-V bias. Under the UV illumination, the total current increases to 150 mA/mm, which means that the photogenerated current is as high as 60 mA/mm. The significantly increased current in the PD under the UV light suggests enhanced 2DEG concentration at the AlGaN/GaN interface through the generation of large amounts of electron–hole pairs (EHPs), which are separated by the built-in field near the heterojunction interface.[20] Compared with the PD without the p-GaN gate, the one with the p-GaN gate shows a one order of magnitude lower photocurrent, suggesting a much less 2DEG formed underneath the p-GaN optical gate. This, on the one hand, might be due to the absorption/reflection of UV light by the p-GaN layer, thus lowering the UV intensity reaching the i-GaN channel; on the other hand, the built-in electric field is reduced near the heterojunction interface due to the p-GaN depletion, resulting in weaker electron confinement; thus, less photogenerated electrons accumulated at the interface. The results indicate that the p-GaN optical gate in the PD can effectively suppress the dark current by depleting the 2DEG underneath while compromising the photocurrent under UV illumination. The conductance of the access region is increased by the enhanced 2DEG concentration with UV illumination. Therefore, reducing both the p-GaN optical gate length and the distance between the electrodes will further increase the photocurrent.

Figure 3 shows the photocurrent and the extracted responsivity (R_i) of the PD as a function of the incident light intensity of the 365-nm UV LED. With a constant 5-V bias across the PD, no photogenerated current can be observed in the device when the light intensity is less than 8×10^{-4} mW/cm^2; above which the photocurrent increases significantly with the increase in the intensity. Therefore, considering the absorption area of the PD to be 800 μm^2, the minimum incident light power is calculated to be $\sim 6.4 \times 10^{-12}$ W (or 6.4 pW) to generate the observable photocurrent in the device, which is believed to be limited by the noise current (dark current dominated). The peak responsivity is determined to be as high as 2×10^4 A/W when the incident light intensity is 0.5 mW/cm^2. Assuming the dark current dominates the noise current, we can calculate the specific

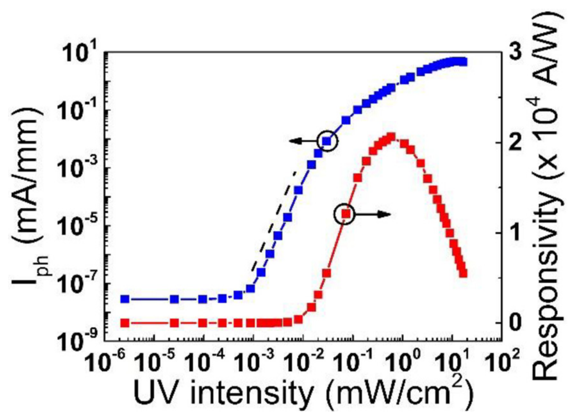

FIG. 3. Photocurrent and responsivity as a function of the incident UV intensity.

detectivity of our PD to be $\sim 1.4 \times 10^{14}$ cm Hz$^{1/2}$ W^{-1} (the device bandwidth of ~50 Hz) using the formula in Ref. 21. As a result of the high responsivity and ultralow dark current in our PD, the detectivity of our PD is in the same order as the highest reported values for GaN-based UV PDs, for instance, 5.3×10^{14} cm Hz$^{1/2}$ W^{-1} for GaN PDs with MSM structures[22] and 1.66×10^{14} cm Hz$^{1/2}$ W^{-1} for PDs with p–i–n structures.[23] The responsivity of a photodetector can be written as[1]

$$R_i = \frac{I_{photo}}{P_{in}} = \frac{\lambda \eta}{hc} q g, \quad (1)$$

where λ is the incident light wavelength, h is the Planck constant, c is the speed of light, η is the quantum efficiency (number of EHPs generated per incident photon), q is the elementary electron charge, and g is the gain of the PD. Assuming that the quantum efficiency is 100%, the gain of the PD can thus be derived to be 6.8×10^4. With a realistic quantum efficiency less than 100%, the calculated gain of the PD could be somewhat higher. The unique device operational principle leads to the much higher estimated gain in our PD than that of conventional GaN PDs with p–i–n (gain ~ 1.8)[24] or MSM structures (~10.5),[4] and commercial Si photodiodes (~0.5) working in this spectral range (Centronic OSD 35-7X).

To illustrate the operation principle and gain mechanism of the PD in this work, we measured the I–V curves of the PD with increasing light intensity of the 365-nm LED illumination [Fig. 4(a)]. It can be observed that under certain incident light intensity, the photocurrent increases linearly with the relatively small bias (less than 0.5 V), while the slope of the I–V curve is dramatically reduced with a further increase in the applied bias. The photocurrent can be modulated by the incident light intensity and tends to be eventually saturated with the applied bias under each light intensity. The PD behaves like a light-intensity-controlled transistor, or the so-called phototransistor. To reveal the gain mechanism of the PD, it is necessary to look into how the photocurrent is formed and what role the photogenerated carriers play in the photocurrent. Under the dark environment, the depletion of the 2DEG underneath the p-GaN optical gate[25] results in high-resistivity of the "channel" and ultralow dark current in the device, as schematically shown in Fig. 4(b). Under UV illumination, EHPs are generated in the i-GaN channel layer by the high excitation energy of the incident photons [E_{photon} (e.g., 3.55 eV for 350 nm) $\geq E_{gap,GaN}$ (3.4 eV)]. Driven by the vertical built-in field, which points from the AlGaN/GaN junction interface to the neutral region of the i-GaN layer, photogenerated electrons in the i-GaN layer are spatially separated from the fixed positively charged ions' center and accumulate at the AlGaN/GaN heterojunction interface,[26,27] becoming 2DEG. The depth of the UV absorption region in i-GaN is estimated to be ~390 nm, according to the absorption coefficient of 365-nm UV light in GaN. As such, the channel region underneath the p-GaN layer is no longer depleted and the 2DEG channel on both sides is connected through the photogenerated electrons, resulting in a low-resistivity conductive path between the electrodes. Consequently, under steady state illumination, infinite electrons are continuously injected from the grounded electrode (source terminal) and flow into the positively biased electrode (drain) by the lateral electric field, thus forming a high photocurrent, as shown in Fig. 4(c). Therefore, the photocurrent comes from the electrons injected from the grounded/source terminal. The photogenerated electrons determine the 2DEG density and thereby the conductivity of the channel. Nevertheless, during a unit time period, the number of electrons that can be collected by the drain is determined by the photogenerated electrons at the 2DEG channel underneath the p-GaN gate, where the 2DEG density is the lowest due to the absorption of UV light in the p-GaN layer. Unlike the photocurrent in the traditional PDs such as p–i–n photodiodes is only from the photogenerated carriers, where the gain can only be obtained through avalanche multiplication,[28] the photocurrent of the PD in this work originates from both the photogenerated carriers and electrically supplied carriers. Hence, an ultrahigh gain can be obtained in these phototransistor-type PDs. It should be noted that the gain in the phototransistor-type PDs is an electrical gain instead of an optical gain in conventional photodiodes. The incident light intensity to the PD works as an optical gate modulating the transistor, and the photogenerated electrons are like gate-bias induced electrons accumulated at the channel (or gate charge), which is ultimately governed by the surface potential of the channel layer. This explains why even though there is no applied bias at the p-GaN, the photocurrent in the two-terminal PD still tends to saturate to some extent. The explanation here also applies to all the phototransistor-type PDs using the AlGa(In)N/GaN heterostructures for carrier conduction.

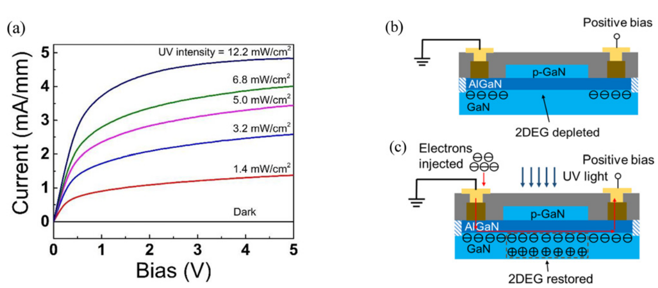

FIG. 4. (a) I–V curves of the PD under different UV intensities illuminated by the 365-nm LED. Schematic illustration of carrier distribution under (b) dark environment and (c) UV illumination.

The photoresponse of the PDs to different incident light wavelengths was measured using a spectroscope with a Xe lamp as the light source. The responsivity of the PD as a function of the wavelength is shown in Fig. 5(a). It can be observed that the cutoff wavelength of the

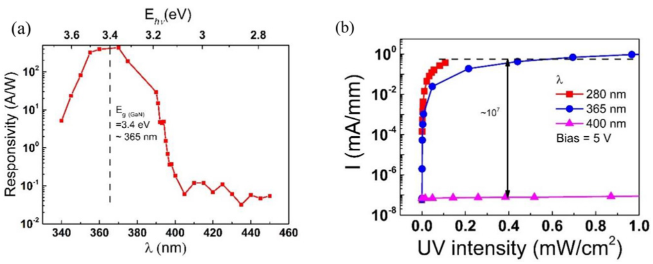

FIG. 5. (a) Wavelength-dependent responsivity of the PD. (b) PD photocurrent as a function of light intensity with LED illumination with center wavelengths of 280 nm, 365 nm, and 400 nm, respectively.

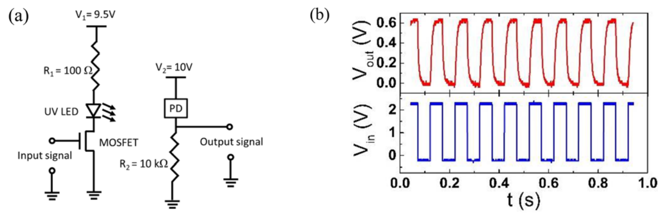

FIG. 6. (a) Schematic of the measurement platform. (b) Time domain photoresponse under the modulation of UV LED with a 20 Hz square signal. The red curve is the voltage measured in the output end in the measurement platform. The blue curve is the voltage on the transistor gate.

PD is ~395 nm, the wavelength where the responsivity drops to 1% of its peak value. The low responsivity in the shorter wavelength range is due to the relatively low incident light intensity from the spectroscope. For the incident light with wavelength larger than 400 nm, no photoresponse was observed in the PD and the calculated responsivity is no longer accurate due to the fluctuation of the measured total current (close to the dark current) and ultralow incident light power. Nevertheless, the results indicate that the PD is blind to the visible spectrum and beyond. To reflect the true capability of the UV-to-visible rejection of the PD, the photocurrent was measured under the illumination of LEDs with center wavelengths of 280 nm, 365 nm, and 400 nm, respectively, as presented in Fig. 5(b). Under the 280-nm UV light illumination, the responsivity can be even as high as $\sim 7 \times 10^4$ A/W. The enhanced UV responsivity under a shorter wavelength is probably due to the absorption/EHP generation in the AlGaN barrier (bandgap ~3.9 eV < 4.4 eV for the 280-nm UV light) in addition to the EHP generation in the i-GaN layer, which increases the 2DEG density. A high UV-to-visible rejection ratio of 1.1×10^7 can be observed at a bias of 5 V, favoring distinctive UV light detection of the device.

To evaluate the frequency response of the PD, a test platform was built to measure the rise and fall times of the PD under the 365-nm LED illumination switched by a Si power transistor, as shown in Fig. 6(a). The LED was switched at 20 Hz, and the photocurrent in the PD was converted to a voltage signal using a resistor in series and recorded with an oscilloscope. The input gate signal of the Si transistor and the output voltage signal of the PD are presented in Fig. 6(b). The high (low) level of the input signal suggests the turn-on (off) of the Si transistor and the LED. The rise time (t_r) and fall time (t_f), defined as 10–90% of the maximum voltage, can be extracted to be 12.2 ms and 8.9 ms, respectively, which are comparable to that of other phototransistor-type GaN PDs. The relatively long time constants compared to MSM PDs are speculated to associate with the persistent conductivity effect in GaN,[15] which can be reduced by applying an additional gate bias on the p-GaN to speed up the charge removal process.[29]

Table I benchmarks the performance of the PDs in this work with the reported state-of-the-art GaN and AlGaN PDs with different structures. It can be observed that our PDs employing a p-GaN/AlGaN/GaN heterostructure on the Si substrate exhibit not only ultralow dark current and high photo-to-dark current ratio, but also high responsivity, high UV-to-visible rejection ratio, and a comparable rise/fall time.

In summary, we have demonstrated high-performance UV PDs using p-GaN/AlGaN/GaN heterostructures grown on the Si substrates. Benefitting from the effective depletion of the 2DEG at the AlGaN/GaN heterojunction interface by the p-GaN optical gate under the dark environment, and the high electrical gain of the high-mobility 2DEG conduction under UV illumination, an excellent photo-to-dark current ratio of over 10^8 and an ultrahigh responsivity of 2×10^4 A/W have been achieved in the device. With cutoff wavelength of around 395 nm, the visible-blind PD exhibits a remarkable UV-to-visible rejection ratio of over 10^7. The persistent photoconductivity resulting in long rise and fall times of several milliseconds is yet to be optimized.

TABLE I. Device performance of photodetectors with different structures based on GaN and AlGaN.

Structure	I_{dark}	I_{ph}/I_{dark}	Responsivity (A/W)	UV/visible rejection ratio	t_{rise}/t_{fall}
GaN PIN Avalanche[23]	3.6×10^{-6} A/cm^2	1×10^4	0.523	10^3	…/…
GaN PIN[30]	8×10^{-10} A/cm^2	1.2×10^4	0.172	10^4	75 μs/110 μs
AlGaN PIN[31]	6×10^{-10} A/cm^2	1×10^4	0.0863	2×10^3	…/…
AlGaN MSM[32]	20 pA	2.6×10^5	…	…	25 ps
AlGaN/GaN 2DEG[17]	10 pA	3.6×10^7	7800	10^6	30 ms/100 ms
GaN MSM[4]	100 pA	1×10^6	3.096	5×10^4	…/…
AlGaN/GaN heterostructure PD[15]	50 nA	5×10^4	0.1	10^4	13.2 ms
AlGaN/GaN HEMT with p-GaN gate[12]	1×10^{-4} mA/mm	5×10^5	6×10^5	4×10^5	2.5 ms/1.9 ms
AlGaN-based HEMT with p-GaN gate[13]	1×10^{-6} mA/mm	1×10^4	3400	2×10^4	…/…
AlGaN/GaN HEMT PD with ITO gate[11]	3×10^{-3} mA/mm	250	2×10^5	2×10^2	…/…
This work	2.8×10^{-8} mA/mm	1.7×10^8	2×10^4	1.1×10^7	12.2 ms/8.9 ms

The operation principle and high-gain mechanisms have been discussed, which can be applied to the PDs with similar device structures. The high-performance UV PDs on Si demonstrated here suggest their enormous potential for cost-effective visible-blind light detection applications.

AUTHORS' CONTRIBUTIONS

Q.L. and H.J. contributed equally to this work.

This work was supported by the Research Grants Council of Hong Kong under General Research Fund Grant No. 16215818. The authors thank Dr. K. Cheng from Enkris Semiconductor, Inc., for providing the epi wafer and the staff of the Nanosystem Fabrication Facility (NFF) and Material Characterization and Preparation Facility (MCPF) at HKUST for their technical support.

DATA AVAILABILITY

The data that support the findings of this study are available from the corresponding author upon reasonable request.

REFERENCES

[1]E. Monroy, F. Omns, and F. Calle, Semicond. Sci. Technol. **18**(4), R33 (2003).
[2]Z. Alaie, S. Mohammad Nejad, and M. H. Yousefi, Mater. Sci. Semicond. Process. **29**, 16 (2015).
[3]B. Butun, T. Tut, E. Ulker, T. Yelboga, and E. Ozbay, Appl. Phys. Lett. **92**(3), 033507 (2008).
[4]S. Y. Chang, M. T. Chang, and Y. P. Yang, IEEE Photonics J. **9**(2), 6801707 (2017).
[5]B. Ren, M. Y. Liao, M. Sumiya, J. Huang, L. J. Wang, Y. Koide, and L. W. Sang, Appl. Sci.-Basel **9**(14), 2895 (2019).
[6]T. Kuan, S. Chang, Y. Su, C. Ko, J. B. Webb, J. A. Bardwell, Y. Liu, H. Tang, W. Lin, Y. Cherng, and W. Lan, Jpn. J. Appl. Phys., Part 1 **42**(9A), 5563 (2003).
[7]L. Li, D. Hosomi, Y. Miyachi, T. Hamada, M. Miyoshi, and T. Egawa, Appl. Phys. Lett. **111**(10), 102106 (2017).
[8]B. Nabet, M. A. Romero, A. Cola, F. Quaranta, and M. Cesareo, in *Proceedings of the 2001 SBMO/IEEE MTT-S International Microwave and Optoelectronics Conference* (IEEE, New York, 2001), p. 57.
[9]V. K. X. Lin, E. Alarcon-Llado, H. H. Kim, S. Arulkumaran, G. I. Ng, A. Ramam, and S. Tripathy, Electrochem. Solid State Lett. **13**(9), H301 (2010).
[10]M. M. Hou, H. Y. So, A. J. Suria, A. S. Yalamarthy, and D. G. Senesky, IEEE Electron Device Lett. **38**(1), 56 (2017).
[11]T. Narita, A. Wakejima, and T. Egawa, Jpn. J. Appl. Phys., Part 1 **52**(1), 01AG06 (2013).
[12]M. Iwaya, S. Miura, T. Fujii, S. Kamiyama, H. Amano, and I. Akasaki, Phys. Status Solidi C **6**(S2), S972 (2009).
[13]A. Yoshikawa, Y. Yamamoto, T. Murase, M. Iwaya, T. Takeuchi, S. Kamiyama, and I. Akasaki, Jpn. J. Appl. Phys. **55**(5), 05FJ04 (2016).
[14]M. Ishiguro, K. Ikeda, M. Mizuno, M. Iwaya, T. Takeuchi, S. Kamiyama, and I. Akasaki, Jpn. J. Appl. Phys., Part 1 **52**(8), 08JF02 (2013).
[15]M. Martens, J. Schlegel, P. Vogt, F. Brunner, R. Lossy, J. Würfl, M. Weyers, and M. Kneissl, Appl. Phys. Lett. **98**(21), 211114 (2011).
[16]S. Kumar, A. S. Pratiyush, S. B. Dolmanan, S. Tripathy, R. Muralidharan, and D. N. Nath, Appl. Phys. Lett. **111**(25), 251103 (2017).
[17]P. F. Satterthwaite, A. S. Yalamarthy, N. A. Scandrette, A. K. M. Newaz, and D. G. Senesky, ACS Photonics **5**(11), 4277 (2018).
[18]H. Jiang, R. Zhu, Q. Lyu, and K. M. Lau, IEEE Electron Device Lett. **40**(4), 530 (2019).
[19]O. Ambacher, B. Foutz, J. Smart, J. R. Shealy, N. G. Weimann, K. Chu, M. Murphy, A. J. Sierakowski, W. J. Schaff, L. F. Eastman, R. Dimitrov, A. Mitchell, and M. Stutzmann, J. Appl. Phys. **87**(1), 334 (2000).
[20]Y. Ohmaki, M. Tanimoto, S. Akamatsu, and T. Mukai, Jpn. J. Appl. Phys. Part 2 **45**(42-45), L1168 (2006).
[21]C. Bao, Z. Chen, Y. Fang, H. Wei, Y. Deng, X. Xiao, L. Li, and J. Huang, Adv. Mater. **29**(39), 1703209 (2017).
[22]L. Liu, C. Yang, A. Patane, Z. G. Yu, F. G. Yan, K. Y. Wang, H. X. Lu, J. M. Li, and L. X. Zhao, Nanoscale **9**(24), 8142 (2017).
[23]Y. Zhang, S. C. Shen, H. J. Kim, S. Choi, J. H. Ryou, R. D. Dupuis, and B. Narayan, Appl. Phys. Lett. **94**(22), 221109 (2009).
[24]Z. Vashaei, E. Cicek, C. Bayram, R. McClintock, and M. Razeghi, Appl. Phys. Lett. **96**(20), 201908 (2010).
[25]G. Greco, F. Iucolano, and F. Roccaforte, Mater. Sci. Semicond. Process. **78**, 96 (2018).
[26]Y. Turkulets and I. Shalish, J. Appl. Phys. **124**(7), 075102 (2018).
[27]Y. Huang, D. J. Chen, H. Lu, H. B. Shi, P. Han, R. Zhang, and Y. D. Zheng, Appl. Phys. Lett. **96**(24), 243503 (2010).
[28]J. B. Limb, D. Yoo, J. H. Ryou, W. Lee, S. C. Shen, R. D. Dupuis, M. L. Reed, C. J. Collins, M. Wraback, D. Hanser, E. Preble, N. M. Williams, and K. Evans, Appl. Phys. Lett. **89**(1), 011112 (2006).
[29]A. M. Armstrong, B. A. Klein, A. A. Allerman, A. G. Baca, M. H. Crawford, J. Podkaminer, C. R. Perez, M. P. Siegal, E. A. Douglas, V. M. Abate, and F. Leonard, Photonics Res. **7**(6), B24 (2019).
[30]W. Z. Xu, Y. T. Shi, F. F. Ren, D. Zhou, L. L. Su, Q. Liu, L. Cheng, J. D. Ye, D. J. Chen, R. Zhang, Y. D. Zheng, and H. Lu, Photonics Res. **7**(8), B48 (2019).
[31]L. Yang, K. Lai, B. Zhang, X. Fu, J. Wang, and W. Wei, Phys. Status Solidi A **212**(3), 698 (2015).
[32]Y. M. Zhao and W. R. Donaldson, IEEE J. Quantum Electron. **56**(3), 1 (2020).